Deciphering of the molecular mechanisms stabilizing the Reovirus entry binding complex

Rita dos Santos Natividade,[1†] Melanie Koehler,[1,2†] Priscila S.F.C. Gomes,[3] Joshua Simpson,[1] Sydni Caet Smith,[4] Diego E. B. Gomes[3], Juliette de Lhoneux,[1] Jinsung Yang,[1] Ankita Ray,[1] Terence S. Dermody,[5] Rafael C. Bernardi,[3*] Kristen M. Ogden,[4,6*] David Alsteens,[1,7*]

[1]Louvain Institute of Biomolecular Science and Technology, Université catholique de Louvain, Louvain-la-Neuve, Belgium
[2]Leibniz Institute for Food Systems Biology at the Technical University of Munich, Freising, Germany
[3]Department of Physics, Auburn University, Auburn, Alabama 36849, USA
[4]Department of Pathology, Microbiology, and Immunology, Vanderbilt University Medical Center, Nashville, Tennessee, USA
[5]Departments of Pediatrics and Microbiology and Molecular Genetics, University of Pittsburgh School of Medicine, and Institute of Infection, Inflammation, and Immunity, UPMC Children's Hospital of Pittsburgh, Pittsburgh, Pennsylvania, USA
[6]Department of Pediatrics, Vanderbilt University Medical Center, Nashville, Tennessee, USA
[7]Walloon Excellence in Life sciences and Biotechnology (WELBIO), Wavre, Belgium
[†]These authors contributed equally to this work.

[*]Address correspondence to Rafael C. Bernardi (R.C.B, rcbernardi@auburn.edu), Kristen M. Ogden (K.M.O, kristen.ogden@vumc.org) or David Alsteens (D.A., david.alsteens@uclouvain.be)

KEYWORDS. Atomic force microscopy, force spectroscopy, reovirus, cell binding, receptors

ABSTRACT (<250 words)

Mammalian orthoreoviruses (reoviruses) have been shown to play a role in triggering the development of celiac disease and, conversely, also own oncolytic properties, making them an interesting tool in cancer therapy. Primary attachment of T1L reovirus to host cellular surface receptors is mainly mediated by the viral trimeric protein σ1, which engages cell-surface glycans, followed by high-affinity binding to JAM-A receptor. It is suggested that this multistep process is accompanied by major conformational changes, but direct evidence is lacking. By combining biophysical, molecular and simulation approaches, we deciphered how the mechanics of viral capsid protein influence virus binding capacity and infectivity. Single virus force spectroscopy experiments further corroborated by *in silico* simulation show that GM2 increases the affinity of σ1 towards JAM-A by providing a more stable contact interface. Alternatively, we demonstrated that conformational changes of σ1 towards an extended rigid conformation also significantly increase avidity to JAM-A. Although its associated lower flexibility impairs multivalent cell attachment, our findings suggest it can enhance infectivity, indicating that a fine tuning of σ1 conformational changes is necessary to successfully orchestrate cell infection. Understanding properties underlying the nanomechanics of viral attachment proteins offers new perspectives in the development of antiviral drugs and the development of improved oncolytic vectors.

Significance statement (50-120 words)

The initial attachment of viruses to cell surface receptors serves as a primary determinant of the success of the infection. However, the dynamics and cooperativity between multiple cell surface receptors are still poorly understood. Focusing on reovirus, an oncolytic human virus, we highlighted how the viruses selected two different roads to a successful infection. First, sialic acids serve as a molecular bridge between the virus and the receptor. Second, reoviruses adopt more extended protein conformers, yielding a more stable molecular complex that favors virus entry. The *in vitro* and *in silico* data presented provide novel biophysical insights into dynamics and outcomes of viral attachment to cell receptors.

Mammalian orthoreoviruses (reoviruses) are nonenveloped, icosahedral viruses (~85 nm) that contain a segmented, double-stranded (ds) RNA genome.[1] While not commonly associated with human disease, reovirus infection appears to trigger the development of celiac disease by disrupting the development of an immunological tolerance to orally ingested gluten.[2] In addition, reovirus shows oncolytic activity across a range of tumour types.[3] Clinical trials have demonstrated that reovirus-based therapeutics are safe and show efficacy when administered in combination with other anticancer treatments.[4, 5] However, a better understanding of reovirus entry mechanisms would help further improve their functionality as therapeutic agents.

To successfully infect host cells, a virus must locate and attach to cell entry receptors that allow uptake and penetration of the cell membrane. For most viruses, this is not a simple one-step procedure, but rather a succession of tightly regulated steps involving binding partners on the surface of the virus and host cell.[6,7, 8] Reovirus binding to cells is predominantly mediated by outer-capsid protein σ1. The σ1 protein is a 150 kDa homotrimeric molecule that assembles into a long fiber protruding from the surface of the viral particle (VP) at the icosahedral fivefold vertices and is partitioned into three domains (tail, body, and head) (Figure 1A).[9,10,11] The N-terminal tail is predicted to form an α-helical coiled-coil, the body domain consists of β-spiral repeats, and the C-terminal head folds into a compact domain composed of eight antiparallel β-strands. For reovirus strain T1L, the glycan binding site resides in the σ1 head domain (Figure 1A, dark blue) and exhibits a preferential affinity for branched glycan GM2.[12] The σ1 head domain also binds to junctional adhesion molecule-A (JAM-A), which serves as an entry receptor for all known reovirus serotypes (Figure 1A, violet).[13, 14,15, 16] After attachment to surface glycans, reovirus virions undergo lateral particle diffusion to bind with higher-affinity to this proteinaceous receptor. We discovered that binding of reovirus strain T3D virions to glycans triggers a conformational change of σ1 to a more extended form, increasing overall avidity for JAM-A.[14] Such a conformational change also has been demonstrated by cryo-electron microscopy for T1L infectious subvirion particles (ISVPs), which are reovirus disassembly intermediates that can be produced *in vitro* by proteolytic digestion.[17,18] However, this change in avidity has not been characterized from a mechanistic and functional point of view.

In this study, we used an innovative approach to characterize, at a single-molecule level, the influence of conformational flexibility in the binding properties of σ1 directly in a cellular context. Combining force distance-based atomic force microscopy (FD-based AFM), single-particle tracking, and steered molecular dynamics (SMD), we determined how T1L VPs or ISVPs or T1L VPs containing σ1 crosslinked at various positions in the σ1 trimer bind to JAM-A and defined how conformational flexibility influences virus binding, diffusion, and infectivity. AFM and SMD results revealed that although GM2 seems not to affect σ1:JAM-A dynamics and force stability, GM2 helps to increase the binding affinity of σ1 towards JAM-A by stabilizing residue pairs contacts at the interface of the complex. While *in vitro* GM2 does not substantially alter reovirus binding to JAM-A, a higher affinity is clearly observed when the σ1 head domains are crosslinked together, both for purified receptor and intact cells. However, although we observed an increase in affinity, this crosslinking also is accompanied by an inhibition of multivalent interactions, as negative cooperativity occurs for multiple bonds in the cellular context.

Overall, our results support the emerging idea of a cooperative role of glycans in stabilizing the complex with its entry receptor and that conformational changes of viral surface proteins to an extended structure promote higher viral receptor binding kinetics. However, some flexibility of σ1 protein is also required to establish multiple binding contacts, which directly affects the capacity of viruses to bind to host cell surfaces and to diffuse as shown by crosslinking σ1 head domain. In the development of new oncolytic vectors, the controlled crosslinking of viral capsid proteins involved in binding to cell entry receptors could open new avenues to improve specific cell targeting.

RESULTS AND DISCUSSION

Probing reovirus T1L binding to purified JAM-A

To evaluate the binding of reovirus strain T1L to JAM-A, we used FD-based AFM and probed the interactions at the single VP level with immobilized purified JAM-A (Figure 1A-C). Virions were immobilized on the tip apex using a polyethylene glycol $(PEG)_{24}$ linker (see Figure S1A for grafting validation) and cyclically approached and retracted from JAM-A (Figure 1B) (see Figure S1B for validation of the JAM-A surface). Specific adhesion events were sorted based on the rupture distance of the rupture event, *i.e.*, at least 5 nm corresponding to the PEG-linker extension, that follows a worm-like chain stretching behavior. [19, 20] First, we analyzed the binding frequencies (BF) of wild-type (WT) T1L VPs to JAM-A and obtained a BF of 11.1 ± 5.0% (mean ± standard deviation [S.D.], N ≥ 4), which is comparable to the frequencies previously observed for reovirus strain T3D.[14] To validate the specificity of the interaction, we injected a JAM-A antibody over the binding surface, which led to a ≈ 6-fold reduction in the BF (Figure S2).

As a conformational change of σ1 was observed for T3D after injection of free sialyloside[14] and for T1L ISVPs by cryo-electron microscopy, we evaluated the BF of T1L VP following glycan engagement, ISVP formation and glycan engagement by ISVP. BF analysis did not reveal significant changes relative to T1L VPs. GM2 injection led to a frequency of 8.9 ± 6.9% for T1L VPs, while T1L ISVPs bound with a frequency of 12.3 ± 3.1% and 12.28 ± 4.4% after addition of GM2 (Figure 1D). These results were surprising in view of the previous results regarding T3D strain,[14] and we conducted a more detailed analysis of the kinetic parameters that characterize the binding energy landscape.

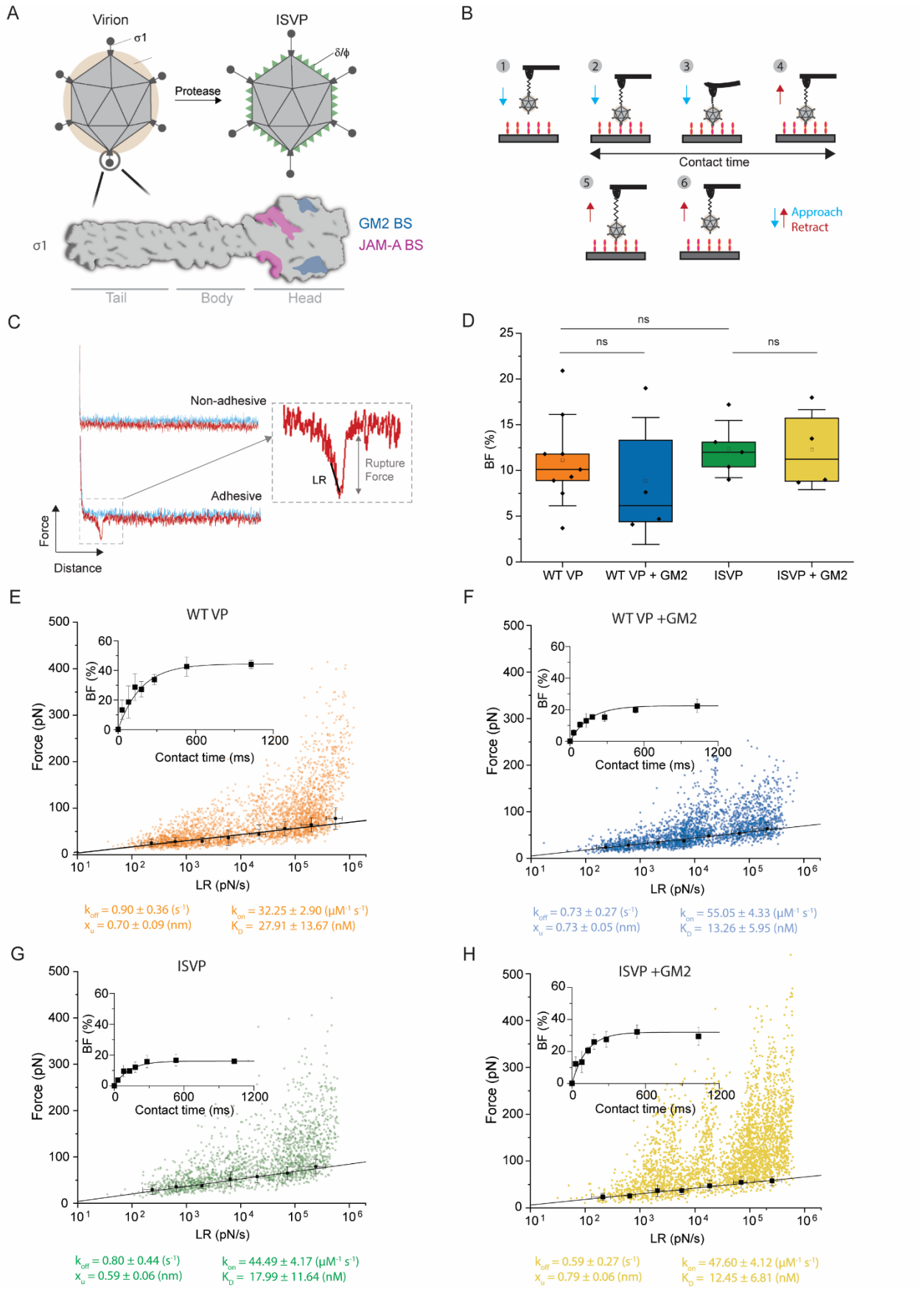
A
Virion
σ1
ISVP
δ/ϕ
Protease
σ1
GM2 BS
JAM-A BS
Tail
Body
Head
B
1
2
3
4
Contact time
5
6
Approach
Retract
C
Non-adhesive
Adhesive
LR
Rupture Force
Force
Distance
D
ns
ns
ns
BF (%)
WT VP
WT VP + GM2
ISVP
ISVP + GM2
E
WT VP
BF (%)
Contact time (ms)
Force (pN)
LR (pN/s)
koff = 0.90 ± 0.36 (s-1)
xu = 0.70 ± 0.09 (nm)
kon = 32.25 ± 2.90 (μM-1 s-1)
KD = 27.91 ± 13.67 (nM)
F
WT VP +GM2
BF (%)
Contact time (ms)
Force (pN)
LR (pN/s)
koff = 0.73 ± 0.27 (s-1)
xu = 0.73 ± 0.05 (nm)
kon = 55.05 ± 4.33 (μM-1 s-1)
KD = 13.26 ± 5.95 (nM)
G
ISVP
BF (%)
Contact time (ms)
Force (pN)
LR (pN/s)
koff = 0.80 ± 0.44 (s-1)
xu = 0.59 ± 0.06 (nm)
kon = 44.49 ± 4.17 (μM-1 s-1)
KD = 17.99 ± 11.64 (nM)
H
ISVP +GM2
BF (%)
Contact time (ms)
Force (pN)
LR (pN/s)
koff = 0.59 ± 0.27 (s-1)
xu = 0.79 ± 0.06 (nm)
kon = 47.60 ± 4.12 (μM-1 s-1)
KD = 12.45 ± 6.81 (nM)

Figure 1. Probing T1L binding to JAM-A on model surfaces. (**A**) Schematic representation of a T1L virion, with the σ1 protein mediating the binding to both GM2 and JAM-A, respectively, highlighted in dark blue and violet. Following proteolytic cleavage, the virion outer capsid is partially removed, generating the ISVP, which involves the release of σ3 subunits and cleavage of μ1 to the δ and φ fragments. In this form, σ1 adopts a more extended conformation. The σ1 trimer consists of three domains: tail, body, and head. (**B**) Schematic of probing a JAM-A coated surface with an AFM tip functionalized with reovirus. First, the tip approaches the JAM-A surface (#1) until contact (#2). The tip continues to approach until a certain force threshold is reached (#3) and is then retracted (#4). In the case of a specific adhesion event, an elongation of the PEG linker is observed (#5) until the bond is ruptured, and the tip moves away from the surface (#6). (**C**) Representative FD curves recorded on the model surfaces showing non-specific and specific adhesion events. Rupture forces are collected from the peak of an unbinding event. Loading rate (LR) corresponds to the slope of the curve just before rupture of the bond. (**D**) Box plot of the binding frequency (BF) between virions and the JAM-A-coated surface, calculated for WT T1L VPs, WT VPs after addition of GM2 (1 mM), T1L ISVPs and T1L ISVPs after addition of GM2 (1 mM). One data point represents the BF obtained for one map of 1024 FD curves. The horizontal line within the box indicates the median, boundaries of the box indicate the 25th and 75th percentiles, and the whiskers indicate the SD. Statistical significance was determined by two-sample t-test. P values for the comparison between WT VPs and WT VPs + GM2 or ISVPs are 0.51 and 0.063, respectively. P value for the comparison between ISVPs and ISVPs + GM2 is 0.94. P values are represented by: ns, $P > 0.05$. (**E-H**) Dynamic force spectroscopy (DFS) plots showing the distribution of the rupture forces as a function of their LR measured between JAM-A and (E) T1L VPs (N = 3468 data points), (F) after injection of GM2 (N = 2514 data points), (G) T1L ISVPs (N = 3326 data points), and (H) ISVPs after injection of GM2 (N = 3099). The solid line represents the fit of the data with the Bell-Evans fit (for simple ligand-receptor bond), which provides average k_{off} and x_u values. The error bars indicate the standard deviation of the mean. Binding frequency is plotted (as inset) as a function of contact time. Data points represent mean BF calculated for each contact time and were fitted using a least-squares fit of a monoexponential decay, providing average values for the k_{on}, and the K_D is calculated using k_{off}/k_{on}. The error bars indicate SD. All data are representative of at least n = 3 independent experiments.

Dynamic force spectroscopy (DFS) experiments were performed by varying the retraction speed to explore a wide range of loading rates (LR, applied force over time) followed by extracting the kinetic parameters describing the free-energy landscape of the interaction between T1L VPs or ISVPs and JAM-A (**Figure 1E-H**). Overall, the probed complexes withstood forces in the range of 25-500 pN across the full range of applied LRs. After extraction of both rupture force and LR for all specific unbinding events recorded for T1L VPs or ISVPs, with or without injection of GM2, the data points were displayed in DFS plots (**Figure 1E-H**). Further, through previously established force histogram analysis (**Figure S3-4**), single rupture events were fitted with the Bell-Evans model,[21, 22] allowing extraction of the unbinding rate (k_{off}) and the distance to transition state (x_u), both extrapolated to zero pulling force (F_0).

From the Bell-Evans fit, we determined a k_{off} of 0.90 ± 0.36 s^{-1} and x_u of 0.70 ± 0.09 nm for the T1L VPs, k_{off} of 0.73 ± 0.27 s^{-1} and x_u of 0.73 ± 0.05 nm after GM2 injection, k_{off} of 0.80 ± 0.44 s^{-1} and x_u of 0.59 ± 0.06 nm for T1L ISVPs, and k_{off} of 0.59 ± 0.27 s^{-1} and x_u of 0.79 ± 0.06 nm after GM2 injection. For T1L VPs, T1L VPs+GM2, and T1L ISVPs+GM2, x_u values were similar. However, for ISVPs we noticed a slight reduction in x_u that we think is attributable to the extended conformation of trimeric σ1 observed by cryo-EM.[17] T1L VPs and ISVPs show a similar k_{off}, while injection of GM2 appears to lead to the same tendency of a slight decrease for both viral particle forms. We also assessed the association rate (k_{on}) by monitoring the effect of contact time on the BF (**Figure 1E-H**,

inset). By fitting the data with a mono-exponential growth model (see methods) assuming that the receptor-bond complex can be approximated by pseudo-first-order kinetics,[23] we obtained the following k_{on} values: 32.3 ± 2.9 $\mu M^{-1} s^{-1}$, 55.1 ± 4.3 $\mu M^{-1} s^{-1}$, 44.5 ± 4.2 $\mu M^{-1} s^{-1}$ and 47.50 ± 4.1 $\mu M^{-1} s^{-1}$ for T1L VPs, T1L VPs after GM2 injection, T1L ISVPs, and T1L ISVPs after GM2 injection, respectively. In these experiments, only GM2 appeared to slightly influence binding to JAM-A. These different behaviors are reflected in dissociation constants (K_D) in the same high-affinity range: 27.9 ± 13.7 nM for T1L VPs, 13.3 ± 6.0 nM after injection of GM2, 18.0 ± 11.6 nM for T1L ISVPs, and 12.5 ± 6.8 nM after injection of GM2 for ISVPs.

Collectively, these results suggest that the affinity of T1L for JAM-A is slightly influenced by sialic acid engagement, for both VPs and ISVPs, which is in good agreement with virus binding assays conducted using CHO JAM-A cells (**Figure S5**). However, this observation is in contrast to what was observed for strain T3D, suggesting that the conformational change may not be as marked for T1L σ1 or beneficial to JAM-A binding.

Influence of GM2 on the T1L σ1:JAM-A complex dynamics

The twofold decrease in K_D observed while probing JAM-A after addition of GM2 suggest that glycans might influence the stability of the σ1:JAM-A complex positively. To further confirm our first observation, a model for the viral T1L σ1 protein trimer complexed with JAM-A in presence and absence of the GM2 glycan was built using comparative modelling in a strategy previously developed.[24] To do so, the structures of T1L σ1 protein trimer in complex with JAM-A (PDB ID 4ODB) and T1L σ1 protein trimer coupled with GM2 (PDB ID 4GU3) were employed. An *in silico* single molecule force spectroscopy approach[25] was then applied to investigate the effects of GM2 on the mechanostability of the complex. In this approach, steered molecular dynamics (SMD) simulations were performed employing NAMD 3[25] in a wide-sampling paradigm. During the pulling simulations, the N-terminal residues of each σ1 monomer were anchored while one of the JAM-A proteins was pulled at constant velocity by its C-terminal residue (**Figure 2A**). The simulations resulted in force vs. extension curves with similar peak-force, but somewhat irregular behaviour, showing clear rupture events at a time, and multi-step events at others (**Figure 2B-C**). For both systems, the existence of multiple shielded events was observed, indicating that the rupture might be happening in multiple small steps. Due to the much higher resolution of the simulations, such multi-step events cannot be investigated *in vitro*.

Building on the force versus extension curves, the Bell-Evans model[22, 26, 27] for the probability distribution of a rupture event, showed very similar behaviour for both systems (**Figure 2D**). The behaviour is in line with the experimental DFS results where injection of GM2 seemed not to affect the force resilience of the complex over the applied LRs (**Figure 1E,F**). However, DFS results also showed that GM2 injection seems to slightly influence binding to JAM-A, reflected by the K_D values. To investigate that, we calculated the potential of mean force (PMF) on the σ1:JAM-A dissociation paths, in presence and absence of GM2, obtained from the SMD simulations. The PMF gives the free-energy profile along the reaction coordinate, capturing the energetics of the studied process.[28] The PMF profile (**Figure 2E**) shows that the dissociation free energy barrier in presence of GM2 is approximately 25% higher than that without GM2,

revealing that GM2 is influencing in the unbinding mechanism by stabilizing the σ1:JAM-A complex.

To better understand why the unbinding free energy barrier is larger in the presence of GM2, we looked at the interface contact surface area between the σ1:JAM-A interface residues, averaged over the SMD trajectories (Figure 2F). This analysis suggested that the contact surface area after the first rupture event is higher in presence of GM2 and that the glycan has a role in maintaining the complex stable for a longer period. Likewise, after the main rupture event, the average force (Figure 2F) shows a higher decrease in absence of GM2. These data corroborate the PMF profiles and the K_D values from the DFS experiments. From an energetic point of view, the work needed to rupture the system becomes larger in the presence of GM2 because the force is applied for a longer time in the unbinding coordinate.

To shed light on how GM2 is influencing the interface, we investigated the σ1:JAM-A interface residues in more detail using the generalized correlation-based Dynamical Network Analysis method.[29] This analysis measures the correlation of the molecular motions between residues. The higher the correlation, the more relevant is their interaction for the stability of the protein complex.[30] The difference in the mean correlation values between the interface residues, before and after the first rupture event (Figure 2G-H), shows no significant difference between the systems (± 0.04). However, the GM2 moieties with α-linked 5-N-acetyl neuraminic acid (Neu5Ac) and N-acetylgalactosamine (GalNAc) display high correlation values with most of JAM-A interface residues (0.40 to 0.70), even after the main rupture event (Figure 2H). This means that the presence of GM2 is contributing to increase the stability of the σ1:JAM-A interface.

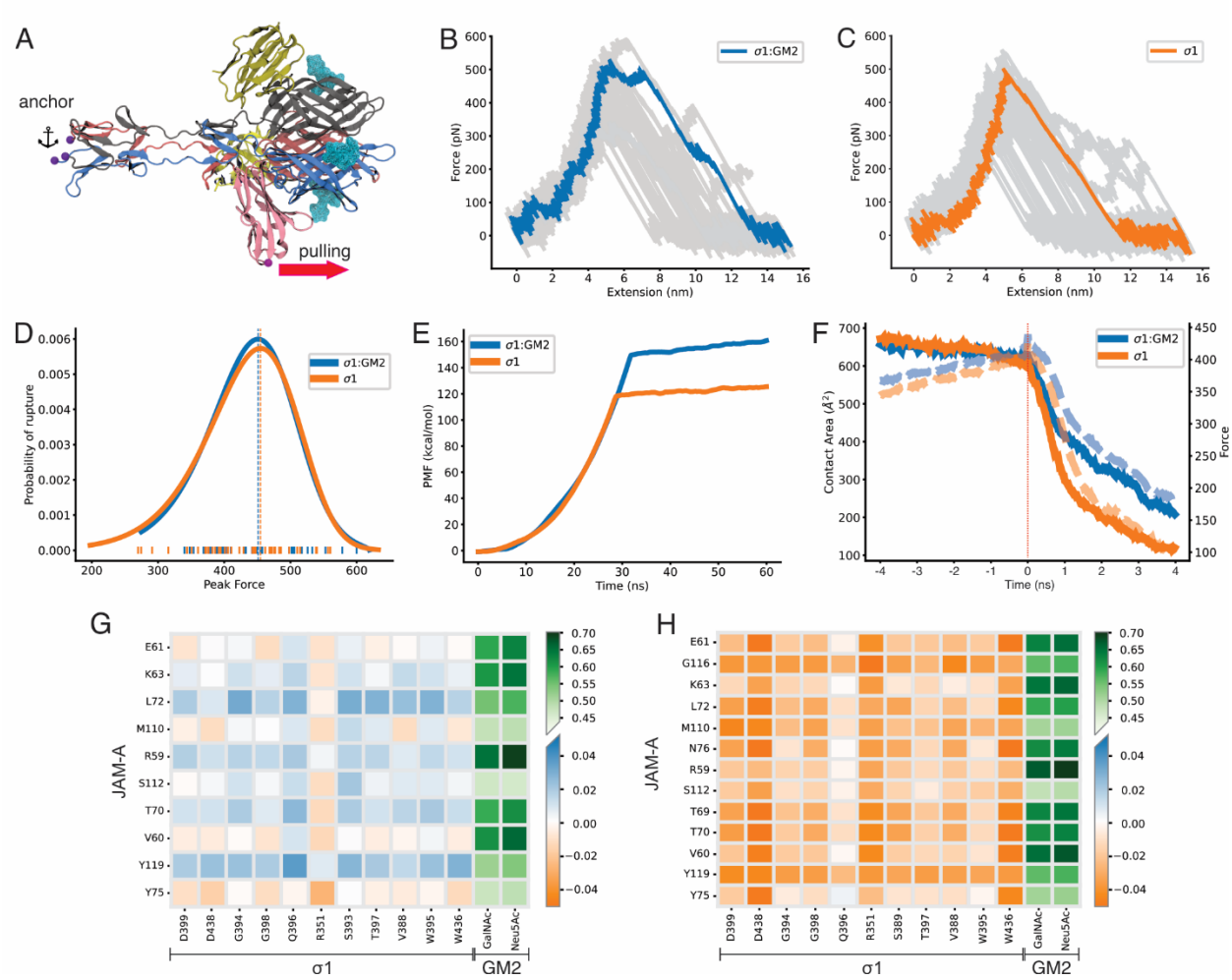

Figure 2. Influence of GM2 on σ1:JAM-A dynamics. For simplicity, the models of JAM-A complexed with σ1 in presence and absence of GM2 are labelled as σ1:GM2 and σ1. (A) Cartoon representation of the tridimensional structure model for the σ1 trimeric protein complexed with three copies of JAM-A and GM2. σ1 monomers are colored in blue, grey and red; JAM-A pulled molecule is colored in pink while the other two molecules are colored in tan; GM2 molecules are represented as surface and colored in cyan. SMD anchor and pulling points are represented as spheres and colored in purple and magenta, respectively. The selected JAM-A molecule was pulled at a constant speed of 2.5 x 10^{-04} nm ps^{-1} with a 0.144 kcal $mol^{-1}Å^2$ spring constant. (B-C) Force versus extension curves for all replicas. Exemplary traces are highlighted in blue and orange. (D) Bell-Evans model for the first rupture peak. (E) Potential of mean force (PMF) versus simulation time. (F) Contact area surface (full lines) and average rupture forces (dashed lines) calculated over the SMD trajectories, 4ns before and after the main rupture event. (G-H) Difference in the mean correlation for the residue pairs in the σ1:JAM-A interface residues (orange to blue) and the glycan:JAM-A interface residues (light to dark green), before (G) and after (H) the main rupture event.

Influence of σ1 crosslinking on σ1:JAM-A complex stability

To precisely control the conformational change associated with the extension of σ1, as undergo for ISVPs particle, and to evaluate the influence of this conformational change on the affinity of σ1 binding to JAM-A, we analyzed the behavior of T1L variant viruses harboring cysteine mutations in σ1. These mutations crosslink σ1 by establishing disulfide bonds between structurally adjacent sites within the tail, body, or head domains.[31] Specifically, we tested T1L viruses containing engineered cysteine residues that crosslink the σ1 tail domain (Tail; N38C), body domain (Body; G287C, V299C), head domain (Head; M332C, S403C), and a fourth variant with crosslinking in the head domain and mutations that abrogate sialic acid binding (HeadΔSA; M332C, S403C, S370P, Q371E) (Figure 3A). While FD-based AFM experiments confirm that Head and HeadΔSA mutants interact with JAM-A with higher BF, as previously observed,[31] this was not observed for the Tail and Body mutants (Figure 3B). We validated the specificity of the interactions using JAM-A antibodies in a blocking assay (Figure S6).

To understand the basis of the different BF observed, we extracted the kinetic parameters using the methodology described above. Specific binding events were displayed on DFS plots (Figure 3C-F), and single-rupture events (Figures S7 and S8) were analysed using the Bell-Evans model. All four mutants displayed lower conformational variability in the bound state, as highlighted by ≈ 2-fold reduction of the x_u (Table S1). In addition, the two head mutants (Head and HeadΔSA) exhibited the lowest k_{off} values, suggesting a stabilized bound state. Further comparison of the different fits (Figure S9) revealed that all four mutants, as well as ISVPs, significantly differ from WT T1L VPs, suggesting that formation of an extended σ1 conformer influences the σ1:JAM-A complex. We also analysed association rates (Figure 3C-F, insets) and observed stabilization of the bound state, marked by a higher k_{on} for both the Head and HeadΔSA mutants (Table S1). Finally, the affinity constant K_D, calculated from the respective k_{on} and k_{off} values, showed that Head and HeadΔSA have higher affinity for JAM-A relative to the Tail and Body mutants, which showed no significant changes relative to WT T1L VPs.

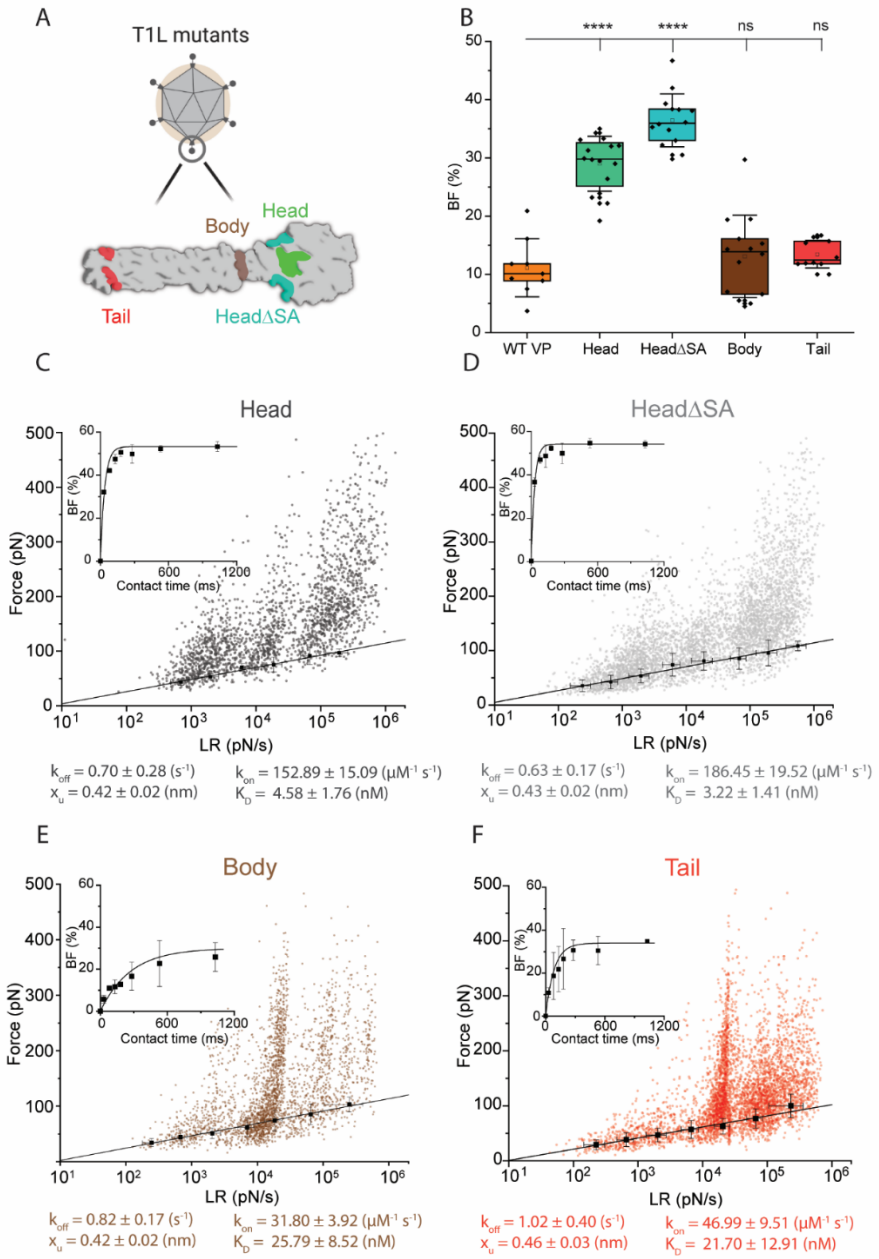

Figure 3. Binding of engineered reovirus mutants to purified JAM-A. (**A**) Schematic representation of a T1L virion and space-filling model of σ1 showing locations of engineered cysteine mutations in the tail, body, and head domains. These mutations result in the formation of disulfide bridges between adjacent monomers within the σ1 trimer, leading to the cross-linking of different regions. (**B**) Box plot of the BF between VPs and JAM-A calculated for WT T1L, Head, HeadΔSA, Body, and Tail. The horizontal line within the box indicates the median, boundaries of the box indicate the 25th and 75th percentiles, and the whiskers indicate the SD. Statistical significance was determined by two-sample t-test. P values for the comparison between WT T1L and Head, HeadΔSA, Body, or Tail are 6.29×10^{-9}, 3.07×10^{-11}, 0.48, and 0.20, respectively. P values are represented by ns, $P > 0.05$; ****$P < 0.0001$. (**C-F**) Dynamic force spectroscopy (DFS) plots showing the distribution of the rupture forces as a function of their loading rate (LR) measured between reovirus and JAM-A, with binding frequency plotted as function of contact time in the inset for engineered mutants (C) Head (N = 2166 data points), (D) HeadΔSA (N = 4317 data points), (E) Body (N = 3005 data points), and (F) Tail (N = 4909 data points). In the DFS plots, the solid line represents the fit of the data with the Bell-Evans fit (for simple ligand-receptor bond). In the binding frequency plots (insets), data points were fitted using a least-squares fit of a monoexponential decay. The error bars indicate SD. All data are representative of at least n = 3 independent experiments.

Taken together, results obtained using the σ1 disulfide mutants indicate that crosslinking of the head domain leads to a more stable bound state (lower K_D), mostly originating from a higher association rate. On the other hand, all mutants exhibit, in the binding free-energy landscape, an energy barrier at a lower distance, meaning that the bound state is capable of accommodating lesser conformational states (Figure S10). Furthermore, this is the distance the molecule has to span between bound and unbound states and indicates its complex mechanical compliance. High values suggest a soft mechanical response, while low values imply a brittle complex. In a more physiologically relevant context, these findings suggest that head domain crosslinking, while improving stability of the complex, yields poor complex compliance.

Deciphering the influence of σ1 conformational change on cell attachment

To determine the influence of σ1 conformational change on attachment to cells, we probed the binding of T1L variants to JAM-A on living Lec2 cells. Lec2 cells were selected for these experiments, as these cells do not express JAM-A and display little sialic acid on the cell surface, leading to poor reovirus binding, as confirmed by a cell binding assay (Figure S11).[32, 33] Lec2 cells that stably expresses JAM-A (Lec2 JAM-A) bind reovirus more efficiently. For the AFM experiments, we co-cultured Lec2 JAM-A cells and Lec2 cells that express the fluorescent construct, (actin:mCherry, H2B:GFP), allowing us to distinguish the two cell lines (Figure 4A). Using FD-based AFM,[19] we simultaneously collected FD curves (Figure 4B) and height and adhesion maps in an area containing adjacent Lec2 JAM-A and Lec2 cells (Figure 4D-F). With this approach we were able to probe both cell types with the same virion to allow direct comparison of the BFs (Figure 4C) and localization of binding events (Figure 4D-F).

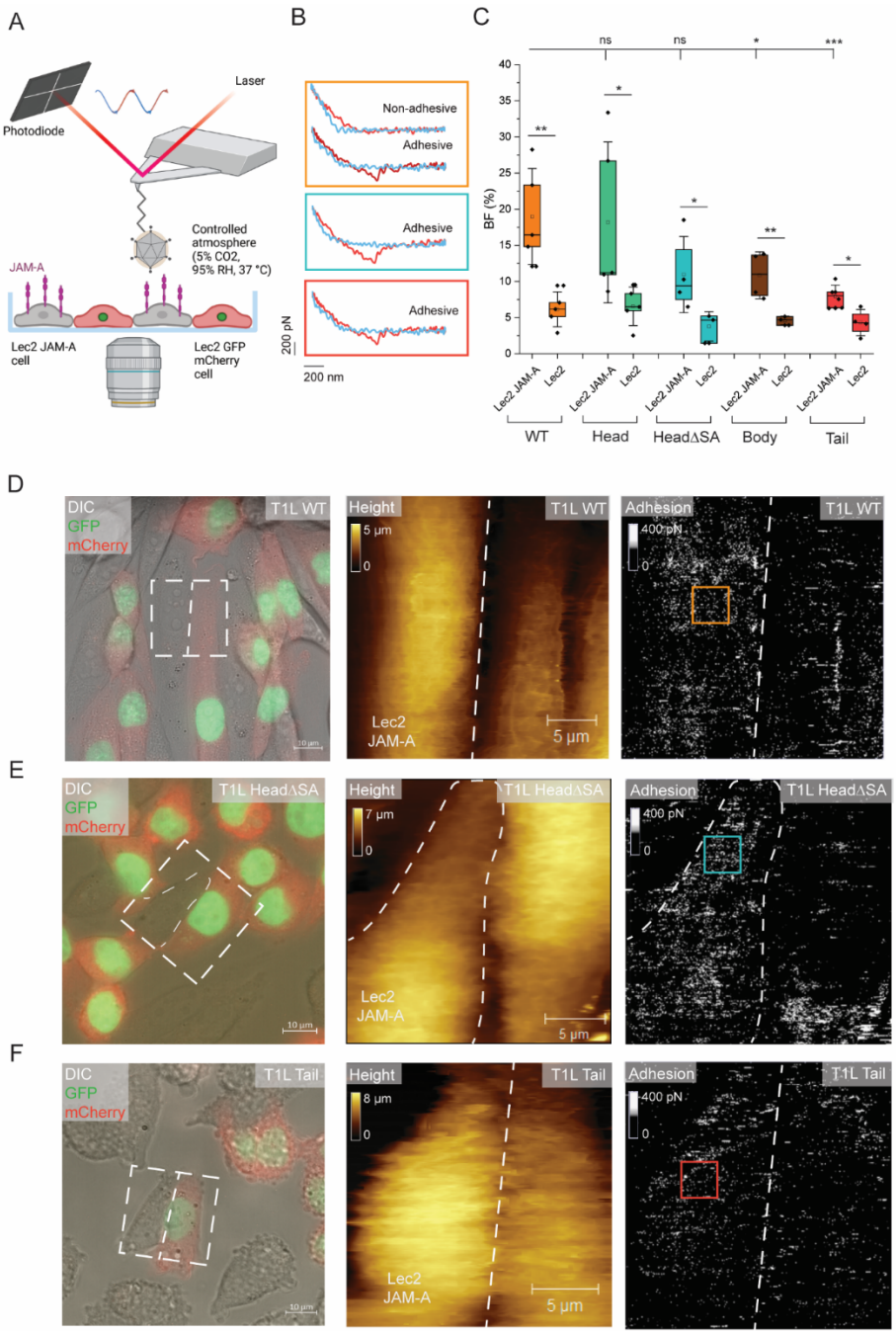

Figure 4. Probing T1L binding to JAM-A on living cells. (**A**) Combined optical microscopy and FD-based AFM of T1L VPs (tethered to the AFM tip) binding to Lec2 JAM-A or Lec2 cells in co culture. (**B**) Representative FD curves recorded by cyclically approaching and retracting the tip to and from the cell's surface, using Lec2 JAM-A cells. FD curves showing non-adhesion or specific adhesion events with either T1L WT, HeadΔSA, or Tail VPs. (**C**) Box plot of the BF between virions and Lec2 or Lec2 JAM-A cells. The horizontal line within the box indicates the median, boundaries of the box indicate the 25th and 75th percentiles, and the whiskers indicate the SD. Statistical significance was determined for the log-transformed BF by two-sample t-test. P values for the comparison between WT T1L VPs and Head, HeadΔSA, Body, or Tail mutants are 0.65447, 0.06227, 0.04274, and 0.00063, respectively. P values are represented by ns, P > 0.05; *P < 0.05; **P < 0.01; ***P < 0.001. (**D-F**) Overlay of DIC and fluorescence channel with the AFM scanned area outlined. FD-based AFM topography image and the corresponding adhesion map collected from the specified scanned area for T1L WT (D), HeadΔSA (E), and Tail (F) VPs. Cartoon in panel A was created in BioRender.com.

For WT T1L VPs and the mutants, the BFs were extracted by pixel counting on the adhesion maps (Figure 4C). For each condition, the BF for Lec2 cells was significantly lower than that for Lec2 JAM-A cells, confirming that most of the probed interactions on Lec2 JAM-A cells are attributable to JAM-A binding. As an additional control, JAM-A Ab was injected to block interactions with σ1, which led to a significant decrease in the BFs for Lec2 JAM-A cells (Figures S12, S13). Overall, the BF of T1L VPs and the Head mutant were slightly higher than those of the other mutants.

To further investigate the capacity of these virus strains to bind JAM-A expressed on living cells, we extracted the binding strength/LR pairs for each specific adhesive event and overlaid these data points on the DFS plots previously obtained on model surfaces (Figure 5). For all five viruses (WT T1L VPs and the four mutants), the extracted forces were in the range 50-500 pN, corresponding to single- and multiple-bond ruptures events. We therefore used the Williams-Evans model (Figure 5B-F, dashed lines)[34] to predict the forces associated with the rupture of simultaneous uncorrelated bonds that are established in parallel. The overlay of the data rupture forces recorded from experiments using living cells, as well as the mean rupture forces extracted from the histograms fitted with multiple Gaussian peak distribution (Figure 5B-F, on the side), revealed agreement between the force of the single bond extracted using living cells and those obtained in experiments using purified JAM-A. Of note, the predictions for multiple interactions coincide well in the case of WT T1L VP and the Body and Tail mutants, but these predictions fail to predict the extracted forces for both the Head and HeadΔSA mutants. Thus, crosslinking of the tail and body domains appears to diminish the capacity to form multivalent bonds, with the vast majority of rupture bonds being single-bond rupture events. These results indicate that in virus attachment to cells, which more faithfully reflects physiological conditions, crosslinking of the σ1 head domain leads to weaker interaction strength than predicted for double or triple bonds. Furthermore, this observation suggests that under polyvalent binding conditions, the most stable bound states are not reached for the head mutants. However, single-bond rupture forces for the head mutants match well with those obtained using model surfaces and, when compared with WT T1L, triple-bond forces appear to be slightly higher for Head and HeadΔSA. This finding highlights an antagonism between higher affinity of σ1 for JAM-A and the flexibility of individual σ1

domains, which influences the stability of multimeric complex formation. The capacity to modulate host cell attachment could be useful in the improvement of oncolytic vectors, as has been done for different strains of adenovirus.[35]

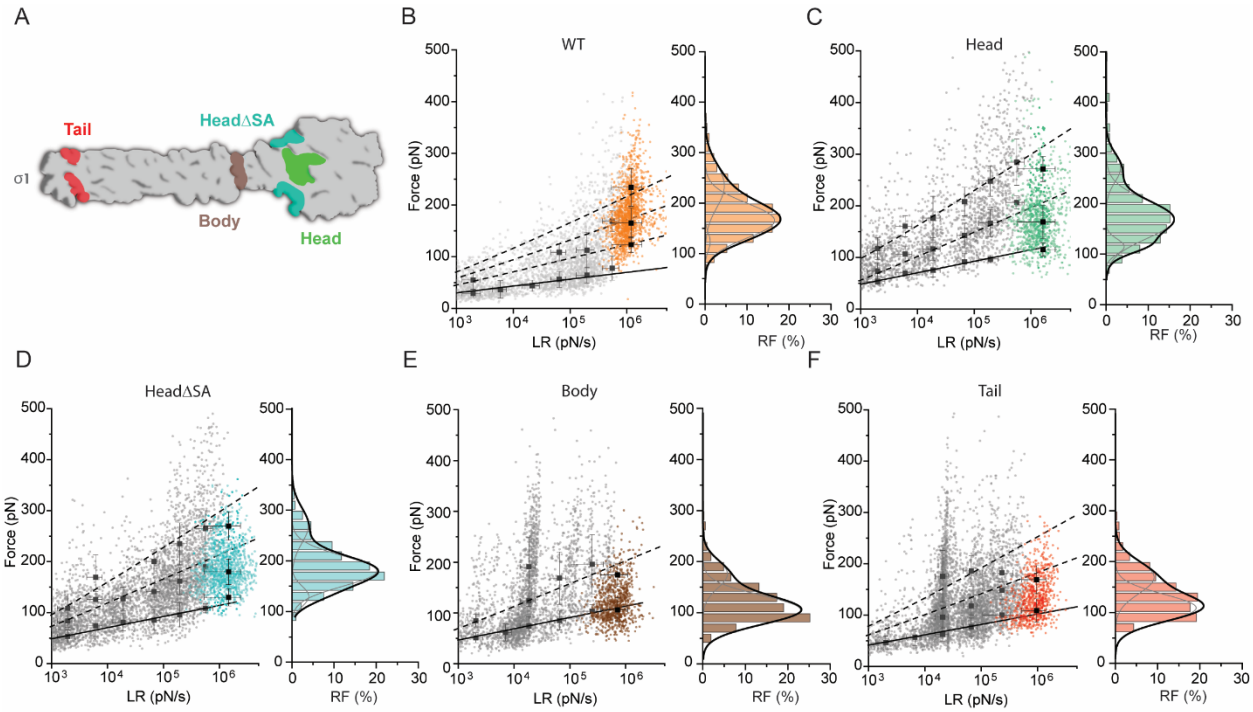

Figure 5. Forces involved in the interaction of virions and JAM-A on living cells. (A) Space-filling model of σ1 showing locations of engineered cysteine mutations in the tail, body, and head domains. (B-F) DFS plots comparing data for virions and JAM-A on model surfaces (grey dots) with overlaid data points from binding experiments using living cells (colored dots) for (B) WT T1L (N = 1546 data points, orange), (C) Head (N = 961 data points, green), (D) HeadΔSA (N = 1227 data points, light blue), (E) Body (N = 857 data points, brown), and (F) Tail (N = 809 data points, red). On the side are shown the respective histograms of the force distribution observed using cells and their relative frequency (RF) fitted with a multi-peak Gaussian distribution.

T1L σ1 mutations affect virus diffusion and uptake into cells

Since σ1 flexibility appears to influence the formation of multivalent bonds with JAM-A, we investigated whether crosslinking the head domain also influences virus binding to and infection of CHO JAM-A cells (Figure 6A). To quantify virus binding, cells were adsorbed with WT T1L, Head, or HeadΔSA at 4 °C to allow attachment but not cell entry. Levels of bound WT, Head, and HeadΔSA virions suggest that crosslinking the σ1 head domain leads to diminished binding to the cell surface. While Head binding is ~18-fold lower than that of WT, HeadΔSA binding is ~2,000-fold lower than that of WT. To quantify the infectivity of WT T1L and the head mutants, cells were incubated with virions at 37 °C, and virus titers were calculated 4 h post-adsorption to allow internalization but not replication and assembly of new virus particles. After standardizing to input virus titers, we observed ~ 3-fold higher infectivity of the Head mutant relative to WT T1L, whereas HeadΔSA displayed ~ 50-fold lower infectivity relative to T1L. Together, these results highlight the importance of σ1 flexibility in binding to host cells, as the rigidity caused by crosslinking the σ1 head domain impairs the capacity of the virion to bind cell-surface receptors. However, the interesting increase in infection efficiency for the Head mutant suggests that a higher affinity for JAM-A provides an advantage to successfully infect cells.

Because there is a close relationship between the capacity of viruses to find and attach to cellular receptors, as well as to diffuse and explore cell surfaces, we determined the diffusion behavior of different viral strains using confocal microscopy and single-particle tracking (SPT) analysis (Figure 6D). Virions fluorescently labeled with Atto488 (mutants) or Alexa488 (WT T1L VP) were injected in a culture with Lec2 JAM-A (Figure 6F-G) or Lec2 cells (Figure S14). Stationary virions or tracks of virions diffusing across the cell surface were selected and used to calculate the mean diffusion speed from experiments using both cell lines (Figures 6E and S14). Mean diffusion speeds observed for WT T1L VPs on cells expressing JAM-A were within 0.01 μm s^{-1} to 0.4 μm s^{-1} (Figure 6E), consistent with heterogeneous behavior ranging from stable attachment to cell receptor-directed diffusion.[36] The Head mutant displayed a slightly lower mean diffusion speed relative to WT T1L VPs, while the Body and Tail mutants displayed increased mean speeds. The Head mutant showed a very small dispersion of the data, with low speeds, suggesting that a vast majority of the virions are immobile.

In contrast, the other mutants diffuse faster than WT T1L VPs, possibly due to a lower affinity for JAM-A (Figure 4) or a diminished capacity to establish multivalent bonds (Figure 5). The reduced diffusion observed for the Head mutants also could be attributable to a more extended σ1 conformer, which might prevent virions from diffusing through the crowded glycoprotein matrix at the cell surface.

To test this hypothesis, we evaluated the hydrodynamic radius of WT and mutant virions, tracking the virions undergoing Brownian motion in a sucrose solution (Figure S15). We observed a similar radius for all strains, between ~ 40-50 nm, in good agreement with previous data,[17] as well as previous dynamic light scattering studies of WT T1L VPs and the mutants.[31] This observation suggests that the σ1 mutations do not influence the rate of free VP diffusion. Overall, the SPT experiments reveal that the T1L mutants diffuse at different speeds only when interacting with the cell membrane, possibly due to a change in σ1 affinity for JAM-A and the capacity to establish multivalent bonds. Results from virus diffusion and infectivity assays suggest that, after encountering and binding to the receptor, Head mutant tends to remain bound and trigger internalization with high efficiency. Thus, we elucidate an intricate σ1:JAM-A mechanism in which flexibility and affinity of the binding partners can be modulated to affect binding and infection of viral particles.

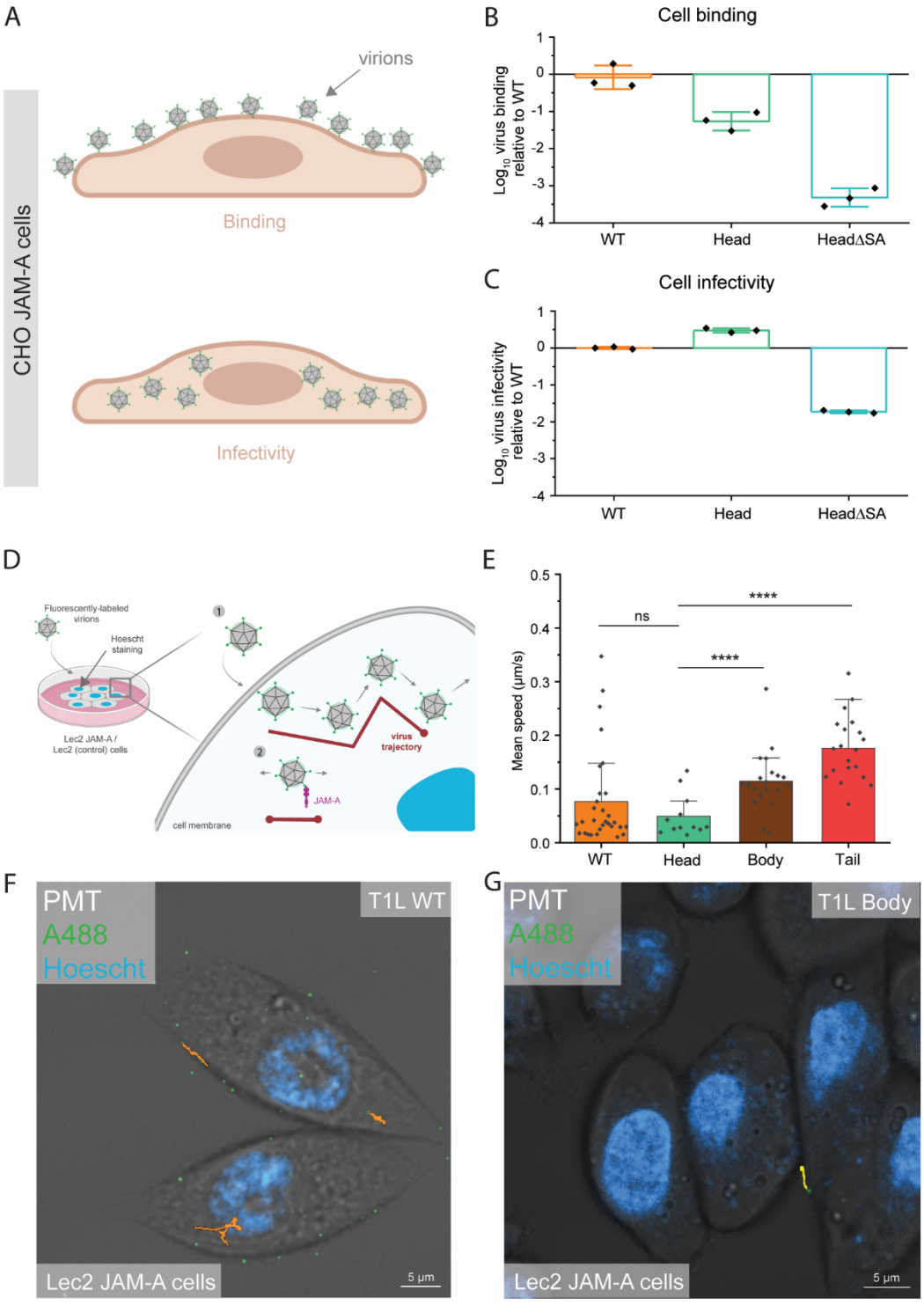

Figure 6. Binding, infectivity, and diffusion of T1L virions on living cells. (A) Schematic of cell binding (conducted at 4°C) and infectivity assays (conducted at 37°C) using CHO-JAM-A cells. (B,C) WT, Head, or HeadΔSA mutants (10^4 particles/cell) were incubated with CHO-JAM-A cells at 4°C for 1 h, and binding relative to WT T1L was determined by quantitative immunoblotting (B) or at 37°C for 4 h, and infectivity relative to WT T1L was quantified by plaque assay (C). Results are expressed in Log_{10} of virus binding or infectivity relative to WT T1L for three experiments. Bars indicate the mean, and error bars represent SD. (D) Representation of an SPT experiment. Virions of WT T1L, Head, Body, or Tail were labeled with Alexa or Atto 488 and adsorbed to Lec2 JAM-A cells. Tracks of particles undergoing lateral particle diffusion (#1), bound to the cell membrane (#2), or stationary were collected. (E) Bar graphs of mean diffusion speed calculated

for WT, Head, Body, and Tail virions following adsorption to Lec2 JAM-A cells. Tracks of at least 10 virions were collected for each condition. The box indicates the mean, and whiskers indicate the SD. Statistical significance was determined for the mean diffusion speed by Mann-Whitney U test. P values for the comparison between Head and WT T1L, Body, or Tail are 0.1997, 2.338×10^{-7}, and 3.489×10^{-9}, respectively. P values are represented by ns, $P > 0.05$; ****, $P < 0.0001$. (F, G) Overlay of images of transmitted light photomultiplier imaging (T-PMT), Hoechst (blue; nucleus of the cells), and Alexa/Atto 488 (green; virions) signals from a time series collected using Lec2 JAM-A cells, where WT T1L VP (F) or Body (G) were added. Examples of tracks belonging to virions interacting with the cell membrane for WT T1L (orange) and Body (yellow) were superimposed. Cartoons in panels A and D were created in BioRender.com.

CONCLUSIONS

The study of the early binding steps of reovirus on cells is of major importance to understand how we can manipulate virus binding and consequent infectivity. Our current understanding of the molecular mechanisms of reovirus binding and cell infection relies mainly on ensemble techniques monitoring either the virus binding or their infectivity, as well as on high-resolution structural data of the molecular complexes associated with those steps. These data suffer from two major limitations: the static nature of the molecular view and the averaging of observations at the scale of the viral population, which does not reflect the stochastic nature of individual behaviours, thus limiting the information that can be extracted including the finest molecular changes. In this context, we used in this study AFM which opens interesting possibilities, allowing us to study the dynamics of virus binding at the single-virus level and even the single-bond level, thus allowing us to extract kinetic and thermodynamic parameters of the established interactions. However, this technique also has its own limitations, in particular the fact that binding is only monitored for very short periods of time, by artificially breaking the bonds under the effect of an external charge after a certain contact time. The force analysis is therefore performed out-of-equilibrium, although providing a robust quantitative analysis of the early interactions established at the cell surface.

In the first part of this study, we used AFM to probe interactions between T1L reovirus and the proteinaceous cell-membrane receptor JAM-A. We have shown that, in vitro, ISVPs only display a slightly enhanced binding kinetics towards JAM-A in comparison with the WT VP, while the addition of GM2 glycans lead to a twofold increase in affinity for VPs binding to JAM-A, as well as a slight increase for ISVPs. To better understand the molecular mechanisms explaining the stabilization of the complex in the presence of GM2 glycan, we performed SMD simulations, and put in evidence a mechanism in which GM2 helps stabilizing the σ1:JAM-A complex for reovirus T1L. Although resulting in both cases to an increase of the affinity towards JAM-A, the underlying molecular mechanism differs from the one previously observed for the T3D serotype, for which the higher affinity was directly linked to a conformational change in σ1. These different behaviours can be linked to the positions of sialylglycan binding sites on the σ1 protein that differ strongly between the two serotypes. In addition, we observed that cross-

linking of the σ1 head domains also leads to a higher affinity towards JAM-A, reminiscent of a behaviour similar to that previously observed for the T3D serotype.[14]

Together, these results shed new light on the dynamics and cooperativity of interactions established by reovirus at the host cell surface receptors. After landing of the viral particle, both glycan engagement and conformational change of the viral capsid can lead to an increase towards the cell entry receptor. These results acquired by single-molecule techniques point towards an importance of σ1 flexibility in the engagement with JAM-A receptors at the cell surface and were confirmed by macroscopic assays such as binding and infectivity tests as well as single-particle tracking. Here, we find that crosslinking σ1 head domain results in enhanced infectivity of viral particles, which is in agreement with SPT data showing lower diffusion speeds on the cell membrane for the same mutant.

This work deepens the knowledge obtained from previous findings and highlights that viral attachment factors play a key role in the early stages of binding. During evolution, viruses or simply different serotypes have selected different strategies to best exploit the early foothold establishes between the virus and the cell surface exposed glycans.

The deep understanding of this mechanism opens new possibilities to control more precisely the binding and entry of reoviruses, opening new therapeutic possibilities.

METHODS

Culture of cell lines. Lec2 cells were purchased from ATCC (CRL-1736). Lec2 cells stably expressing actin-mCherry and H2B-GFP, and Lec2 cells stabling expressing JAM-A were previously established.[14] Lec2 cells were cultured in MEM α nucleosides medium (Gibco, the Netherlands). CHO-K1 (CHO) cells were obtained from the ATCC (CCL-61), and CHO cells stably expressing actin-mCherry and H2B-GFP, and CHO cells stably expressing JAM-A were previously established.[14] CHO cells were cultured in Ham's F12 medium (Sigma-Aldrich, United Kingdom). Both media were supplemented to contain 10% FBS (Gibco, USA), 100 units.ml^{-1} penicillin, 100 µg mL^{-1} streptomycin (Sigma-Aldrich, USA), 2 mM L-Glutamine (Sigma-Aldrich, USA) and 100µg.mL^{-1} Normocin (InvivoGen, France). Spinner-adapted L929 fibroblasts (L cells) were grown in suspension culture in Joklik's minimum essential medium (US Biological) supplemented to contain 5% FBS (Gibco, USA), 2 mM l-glutamine (Corning, USA), 100 U/ml penicillin and 100 µg mL^{-1} streptomycin (Corning, USA), and 25 ng mL^{-1} amphotericin B (Corning, USA). All cells were grown at 37 °C in a humidified atmosphere with 5 % CO_2.

Viruses. Laboratory stocks of parental reovirus strain rsT1L and σ1 cysteine mutants were engineered using plasmid-based reverse genetics, as described.[31] Viral titers were determined by plaque assay using L cells, as described.[37] VPs were purified from infected L cells by deoxycholate permeabilization, Vertrel XF (DuPont) extraction, and CsCl gradient centrifugation, as described.[18] ISVPs were prepared by treatment of purified virus particles with chymotrypsin (Sigma-Aldrich, USA).[38]

Labelling of the reovirus with fluorescent dye. Reovirus virions were labeled with Atto 488 succinimidyl ester (Atto 488-NHS; ATTO-TEC, Germany) as described.[39, 40] Reovirus particles (3 x 10^{12}) were suspended in a freshly prepared 0.05 M sodium bicarbonate (pH 8.5) to a final volume of 499 µL. Then, 1 µL of 10 mM Atto 488-NHS (stored in anhydrous dimethyl sulfoxide (Sigma-Aldrich, Germany)) was added, and the mixture was incubated at RT for 90 min in the dark and while gently rocking. VPs were dialyzed against phosphate-buffered saline (PBS) (Sigma-Aldrich, United Kingdom) buffer at 4°C using Slide-A-Lyzer™ MINI Dialysis Device Kit, 10K MWCO, 0.1 mL (Fisher Scientific, IL, USA). The PBS was replaced after 1 h, 2 h, 6 h and incubated overnight. Another

dialysis step followed, using a dialysis tubing cellulose membrane (Sigma-Aldrich, MO, USA) with a molecular weight cut off of 14000 $g.mol^{-1}$, by immersing it in PBS overnight. Finally, an Amicon Ultra-0.5 centrifugal filter unit (Millipore, Germany) was used to collect the virus particles, which were stored at 4 °C until further use.

Functionalization of AFM tips. AFM tips were functionalized using previously described protocols.[41, 42] Briefly, the tips were first rinsed with chloroform (Sigma-Aldrich, France) for 5 min and then cleaned with UV radiation and ozone (UV-O) (Jetlight, CA, USA) for 15 min. A desiccator was flooded with argon gas and two small plastic trays were placed inside. The tips were placed inside the desiccator, 30 µL of APTES and 10 µL of triethylamine were pipetted separately into the trays and the desiccator was closed. After 2 h of incubation, the trays with APTES and triethylamine were removed and the desiccator was flooded with argon gas for 10 min. The AFM tips were then left to "cure" the APTES coating for at least 2 days. After amino-functionalization, the AFM tips were coupled with flexible PEG linkers as follows. The tips were immersed for 2 h in a solution containing 1 portion of Ald-Ph-PEG_{24}-NHS ester (3.3 mg) (Broadpharm, CA, USA) in chloroform (0.5 mL) (Sigma-Aldrich, Germany) and triethylamine (30 µL) (Sigma-Aldrich, Germany), followed by cleaning for 5 min in chloroform three times. After letting the tips dry, they were placed on Parafilm in a polystyrene Petri dish and stored in an ice box. Next, 100 µL of virus solution (10^9 particles mL^{-1}) were pipetted onto the tips and 2 µL of freshly prepared sodium cyanoborohydride solution (~6 % [wt/vol] in 0.1 M $NaOH_{aq}$) was added to the virus droplet, followed by incubation for 1 h at 4 °C. Then, 5 µL of ethanolamine (1 M [pH 8.0]) (Sigma-Aldrich, Germany) were added to the droplet, mixed carefully and the tips were incubated in this solution for 10 min at 4 °C. The tips were rinsed three times in ice-cold virus buffer (150 mM NaCl, 15 mM $MgCl_2$, 10 mM Tris [pH 7.4]). Finally, the tips were placed in individual wells of a multiwell-plate, in 2 mL of virus buffer. The tips were stored at 4 °C until further use.

Preparation of JAM-A-coated model surfaces. His-tagged JAM-A protein (Bioconnect, Canada) was immobilized using NTA-His_6 binding chemistry.[43] Gold-coated surfaces were rinsed with ethanol, dried with a low nitrogen flow and cleaned with UV-O for 15 min. The surfaces were incubated overnight in an ethanol solution containing 0.05 mM

NTA-terminated (10 %) and PEG-terminated (90 %) alkanethiols. The next day, the surfaces were rinsed with ethanol, dried with gas nitrogen and incubated in a 40 mM aqueous solution of $NiSO_4$ (pH 7.2) for 1 h. After rinsing the surfaces with milliQ water and drying with gas nitrogen, they were placed on a Teflon surface and incubated with JAM-A protein (0.1 mg mL^{-1}) for 1 h. Finally, the surfaces were rinsed ~10 times with PBS and stored at 4 °C until further use, always keeping the surfaces hydrated.

FD-based AFM on model surfaces. Force distance (FD) -based AFM experiments were performed at room temperature, in PBS, using virus-functionalized MSCT-D probes (Bruker, Germany). Cantilever spring constants were calculated using thermal tune method,[44] with values within the range of 0.023 – 0.043 N m^{-1}. Force-Robot300 (Bruker, Germany) operated in the force volume (contact) mode was used to conduct these experiments. JAM-A grafted model surfaces were mounted on a piezoelectric scanner using a magnetic carrier. For all experiments, areas of 5 x 5 µm were scanned, with 32 x 32 pixels resolution (corresponding to 1,024 FD curves) and a ramp size set to 500 nm. The maximum force was set to 500 pN and the approach velocity was kept constant at 1 µm s^{-1}.

Dynamic force spectroscopy (DFS) experiments were conducted with no surface delay and by varying the retraction velocities, set to 0.1, 0.2, 1, 5, 10, and 20 µm s^{-1}, in order to probe a wide range of loading rates. Kinetic on-rate (k_{on}) measurements were performed by adding different hold times (0, 50, 100, 150, 250, 500 and 1000 ms), allowing the tip to stay in contact with the surface for different periods of time.

To monitor the effect of sialic acid addition, DFS and k_{on} experiments were conducted in the same manner as described above, followed by the injection of 1 mM GM2 (Sigma Aldrich, Germany). One map was collected before the addition of GM2 and the same area was scanned after.

Surface blocking was performed as an independent negative control experiment, to ensure specific interaction between the virus and the sample; measurements were collected before and after adding JAM-A antibody (Sigma-Aldrich, Germany) at a concentration of 100 µg mL^{-1} to the sample to block JAM-A binding. A retraction velocity

of 1 μm s^{-1} was kept constant, no surface delay was set and the same sample area was probed several times, using the same tip.

Depending on the instrument used, either JPK Data Processing (version 6.1.149) (Bruker, Germany) or NanoScope analysis software (v1.7, Bruker) (Bruker, Santa Barbara, CA, USA) was used for analysis. FD-curves were fitted with the worm-like chain model for polymer extension.[45] Regarding DFS experiments, loading rates were determined using the slope of the force-time curves and rupture forces were extracted. These results were displayed in DFS plots with Origin software (OriginPro 2021, 9.8.0.200), also used to fit the histograms of rupture force distributions for distinct LR ranges, applying various force spectroscopy models, as described.[19,46] For kinetic on-rate analysis, the binding frequency (BF; fraction of curves that displayed a binding event) was determined for the different hold times (t; the time the tip is in contact with the surface). Those data were fitted and K_D calculated as described.[47]

MD simulations and analyzes. The tridimensional structure of the complex T1L-σ1:JAM-A coupled with GM2, for simplicity called σ1(GM2):JAM-A, was modelled with Modeller v.10.1,[48] using as templates the crystallographic structures of T1L-σ1 in complex with GM2 (PDB id 4gu3)[12] and T1L-σ1 in complex with JAM-A (PDB id 4odb).[16] The system was initially built with GM2 molecules, which were subsequently removed from the model to create the σ1:JAM-A system. Parameters for glycan molecules and model structures preparation were obtained through the CHARMM-GUI web interface.[49] The complex was solvated using TIP3 water model[50] and the total charge neutralized using NaCl 0.15 mol L^{-1} ion concentration. Simulation parameters were obtained from QwikMD,[51] and all molecular dynamics (MD) simulations were performed employing the NAMD 3 package.[25] Simulations were carried out at the local NVIDIA DGX-A100-based cluster nodes at Auburn University. The CHARMM36 force field[52] was used to describe the system and the simulations were performed under periodic boundary conditions. A distance cut-off of 12.0 Å was applied to short-range nonbonded interactions, whereas long-range electrostatic interactions were treated using the particle-mesh Ewald (PME) method.[53] Before the steered molecular dynamics (SMD) simulations, the systems were minimized and equilibrated in three steps: (i) energy minimization for 5000 steps followed by a short 1.0 ns MD using an NVT ensemble, with restraints

(100kcal mol^{-1} $Å^2$) on backbone and sugar atoms (when present); (ii) 1.0 ns MD in an NpT ensemble with restraints (10kcal mol^{-1} $Å^2$) on backbone and sugar atoms (when present); unrestrained 1ns MD. The temperature was maintained at 300 K using Langevin dynamics for temperature and pressure coupling, the latter kept at 1 bar for NpT MD simulations. The time step of integration was chosen to be 4 fs for all SMD production simulations performed, and 2 fs for all equilibration runs. SMD simulations were performed in 40 replicas for each system, with a total of 60ns each replica. In total, nearly 5.0 μs of MD were performed. During SMD, the N-terminal residue of each T1L monomer was anchored while the C-terminal residue of one of JAM-A molecules was pulled at a constant speed of 2.5 x 10^{-04} nm ps^{-1} with a 0.144 kcal mol^{-1} $Å^2$ spring constant.

The Potential of mean force (PMF) was calculated over the dissociation path obtained from the SMD simulations, considering the distance between the anchor and pulling points as the reaction coordinates. The method uses the Jarzynski's equality to connect non-equilibrium properties (SMD simulations) with equilibrium properties. The PMF was estimated by accumulating the logarithm of the exponential average of the work over all replicas.[28]

The most probable loading rate (LR) for the rupture events was determined with a Kernel Density Estimator (KDE) with the bandwidth chosen through the Silverman estimator.[54] The LR was used to fit the rupture force histograms with the Bell-Evans (BE) model to determine the most probable rupture force, the distance to the transition state Δx0, the natural off-rate at zero force $koff_0$, and the energy barrier ΔG^{++} in units of k_BT at T = 300 K.

Mean correlation between σ1:JAM-A interface residues was carried out using Dynamical Network Analysis[29] and VMD.[55] In Dynamical Network Analysis, a network is defined as a set of nodes that represent amino acid residues, and the node's position is mapped to that of the residue's α-carbon. Edges connect pairs of nodes if their corresponding residues are in contact, and 2 non-consecutive residues are said to be in contact if they are within 4.5 Å of each other for at least 75% of analyzed frames. The interface residues between σ1 and JAM-A were defined in a radius of 10 Å between

nodes in each molecule. The analysis was carried out 5ns before and 2ns after the first peak force.

The intermolecular surface contact area ($Å^2$) was calculated using in-house scripts based on Connolly's solvent accessible surface algorithm.[56]

All charts were generated using in-house python scripts. The protein image was rendered using VMD.

FD-based AFM and fluorescence microscopy on living cells. AFM (Bioscope Resolve, Bruker, Santa Barbara, CA, USA), operated in the PeakForce QNM mode (Nanoscope software v9.2), coupled to an inverted epifluorescence microscope (Zeiss Observer Z.1, Zeiss, Germany) were used to acquire correlative images and to conduct FD-based AFM. The AFM was equipped with a 150-µm piezoelectric scanner. A 40x oil objective (NA = 0.95) was used. Cells were kept in MEM α, nucleosides medium (Gibco, the Netherlands) and a cell-culture chamber was used to maintain temperature at 37 °C ± 1 °C. The chamber was infused at 0.1 L min^{-1} with a gas mixture supplemented with 5 % CO_2 and 95 % relative humidity. Vacuum, incorporated into the AFM sample plate, was used to fix the Petri dish where the cells were kept. PFQNM-LC pre-calibrated cantilevers (Bruker, Santa Barbara, CA, USA) were used and their sensitivity was calculated through thermal noise method. The cantilevers were oscillated at 0.25 kHz in PeakForce tapping mode, with an amplitude of 750 nm. AFM images were taken by probing an area of 22-30 µm at imaging forces of 500 pN and a scan frequency of 0.125 Hz. The sample was scanned using 256 pixels per line (256 lines). AFM images and FD-curves were analyzed with NanoScope analysis software (v1.7, Bruker), Origin software (OriginPro 2021, 9.8.0.200), ImageJ (v1.52e) and Gwyddion (version 2.58). FD-curves with peaks corresponding to adhesion events were analyzed with NanoScope analysis and Origin software. Loading rates were determined using the slope of the force-time curves. Optical images were analyzed with Zen Blue software (version 3.2, Zeiss, Germany).

As independent negative control experiments, JAM-A antibody (at 50 µg mL^{-1}; Sigma-Aldrich, Germany) was added to the sample in order to ensure specific interaction

between the virus and the sample. Correlative images were acquired before and after adding the antibody and all the experimental parameters were kept the same.

NanoScope analysis software (v1.7, Bruker) and Origin software were used to analyze FD-curves showing adhesion events. AFM images were analyzed with NanoScope analysis software and Gwyddion. The binding frequency was calculated through pixel counting using ImageJ. Optical images were analyzed with Zen Blue software.

Cell binding assay. Virus binding to cells was quantified as described.[31] Lec2, Lec2 JAM-A, or CHO JAM-A cells (5×10^5) were aliquoted into Eppendorf tubes on ice. Dilutions of purified WT VP, WT VP + 1 mM GM2, or ISVP (10^4 particles/cell) were prepared in cold medium. In the case of Lec2 and Lec2 JAM-A cells, dilutions of 5×10^4 (5X) and 2.5×10^5 (25X) particles/cell also were prepared in cold medium. Cells were pelleted and adsorbed with virus, medium (mock), or medium + 1 mM GM2 at 4°C for 1 h. Following adsorption, cells were pelleted and washed twice prior to addition of radioimmunoprecipitation assay (RIPA) buffer supplemented with 1mM phenylmethylsulfonyl fluoride (PMSF). Samples were boiled with SDS sample buffer and resolved on a 10% Mini-Protean TGX precast protein gel (Bio-Rad). Proteins were transferred to nitrocellulose membranes, which were blocked in Pierce protein-free (PBS) blocking buffer, then incubated with 1:2,000 diluted mouse monoclonal anti-GAPDH (Invitrogen) and 1:500 diluted rabbit polyclonal anti-reovirus serum. Membranes were washed in PBS + 0.1% Tween20 and incubated with anti-rabbit IRDye680LT and anti-mouse IRDye800CW antibodies (LI-COR) diluted 1:15,000 in PBS + 0.1% Tween20 + 5% nonfat dry milk. After washing, membranes were scanned using a ChemicDoc MP imaging system (BIO-RAD). Protein band intensity was quantified using Image Lab 6.1 (BIO-RAD) and normalized to that of WT VP.

Cell infectivity assay. To quantify the infectivity of bound virus, dilutions of purified WT VP, Head VP, or HeadΔSA VP (10^4 particles/cell) were prepared in cold medium. CHO JAM-A cells (5×10^5) were aliquoted into Eppendorf tubes on ice and adsorbed with virus at 4°C for 1 h. Following adsorption, cells were pelleted and washed twice. RIPA buffer was added to cells in half of samples, and they were processed as described above in the cell binding assay, to quantify virus adherence to the cell surface. Cells in the other

half of samples were resuspended in pre-warmed medium and incubated for 4 h at 37 °C to permit infection but not a complete replication cycle. The cells were then lysed by two rounds of freezing at -80°C and thawing to release virus, and virus titer in the samples was determined by plaque assay on L cells. Sample titer was adjusted based on input titer for each virus. Protein band intensity and infectivity titers each were quantified and normalized to those of WT VP.

Single-particle tracking. In all experiments, tracks of reovirus virions labeled with Atto 488 or Alexa 488 were collected. Lec2 JAM-A and Lec2 cells were cultured separately and kept in MEM α, nucleosides medium (Gibco). Cells were incubated at 4°C for 30 min prior to the experiment to ensure binding of virus particles without internalization, and DNA was stained with Hoechst33342 (ThermoFisher, USA) as per supplier protocol. Virions of WT T1L, Head, Body and Tail were added to the samples and tracks of particles that were static, surface bound or trafficking on cells were collected. A Zeiss 980 confocal laser-scanning microscope (Zeiss GmbH, Germany) was used to acquire time series and Z-stack images. This microscope is equipped with 40x water objective (NA = 0.95), argon, helium-neon lasers, a heated stage, CO_2 supply, and GaAsP-PMT detectors. Images were processed using Zen Blue software (version 3.2, Zeiss, Germany) and time series images were exported as TIFF files for import into ImageJ (v1.52e). Individual viruses were tracked using the Trackmate plugin, and the trajectory data exported to Microsoft Excel for further analysis. Behaviors of at least 10 virions per sample were analyzed by extracting their diffusion rate. Population statistics were graphed using Origin software (OriginPro 2021, 9.8.0.200). In order to assess the free diffusion rate of the reovirus T1L WT and mutants, virions were added to a ~13.3 % or 16 % sucrose solution. The individual tracks obtained were assumed to be undergoing Brownian motion and the retrieved diffusion speeds were used to estimate the hydrodynamic radius through input into the Stokes–Einstein equation. All sucrose experiments were conducted at RT.

Statistical analysis. JMP® Statistical Software (JMP® Pro 16.0.0) and https://www.statskingdom.com/ were used to perform statistics tests. P values are represented by: ns, $P > 0.05$; *$P < 0.05$; **$P < 0.01$; ***$P < 0.001$ and ****$P < 0.0001$. Statistical significance of BF values was assessed by conducting Two-Sample t-Tests. To achieve

a normal distribution of the results, a log 10 of the BF was used for statistical analysis of the data from experiments with living cells. Statistical significance of mean diffusion speed values, which did not follow a normal distribution, was assessed by conducting Mann-Whitney U tests.

ACKNOWLEDGMENTS

This work was supported by the Université catholique de Louvain and the Fonds National de la Recherche Scientifique (FRS-FNRS). This project also received funding from the FNRS-Welbio (Grant # CR-2019S-01) and the National Institutes of Health (R01 AI155646 to K.M.O. and R01 AI174526 to T.S.D.). The funders had no role in study design, data collection and analysis, decision to publish, or preparation of the manuscript. M.K. and J.S. are Postdoctoral Researchers, and D.A. Research Associate at the FNRS. This work was supported by the National Science Foundation under Grant MCB-2143787 (CAREER: In Silico Single-Molecule Force Spectroscopy). We thank Auburn University and the College of Sciences and Mathematics for the computational resources provided by Dr. Bernardi faculty startup funds.

AUTHOR ORCIDS

David Alsteens: https://orcid.org/0000-0001-9229-113X
Terence S. Dermody: https://orcid.org/0000-0003-1853-8741
Melanie Koehler: https://orcid.org/0000-0003-3042-1749
Rita do Santos Natividade: https://orcid.org/0000-0002-0123-4760
Kristen Ogden: https://orcid.org/0000-0002-2670-4335
Sydni Caet Smith: https://orcid.org/0000-0002-3217-0843
Priscila S. F. C. Gomes: https://orcid.org/0000-0001-7370-9596
Diego E. B. Gomes: https://orcid.org/0000-0003-4855-040X
Rafael C. Bernardi: https://orcid.org/0000-0003-0758-2026
Juliette de Lhoneux: https://orcid.org/ 0000-0003-1150-758X
Jinsung Yang: https://orcid.org/0000-0002-9731-1002
Joshua Simpson: https://orcid.org/0000-0002-8823-8130
Ankita Ray: https://orcid.org/0000-0002-5059-9598

COMPETING INTERESTS

The authors declare no competing interests.

REFERENCES

1. Guglielmi, K.; Johnson, E.; Stehle, T.; Dermody, T., Attachment and cell entry of mammalian orthoreovirus. *Reoviruses: Entry, Assembly and Morphogenesis* **2006**, 1-38.
2. Bouziat, R.; Hinterleitner, R.; Brown, J. J.; Stencel-Baerenwald, J. E.; Ikizler, M.; Mayassi, T.; Meisel, M.; Kim, S. M.; Discepolo, V.; Pruijssers, A. J., Reovirus infection triggers inflammatory responses to dietary antigens and development of celiac disease. *Science* **2017,** *356* (6333), 44-50.
3. Phillips, M. B.; Stuart, J. D.; Stewart, R. M. R.; Berry, J. T.; Mainou, B. A.; Boehme, K. W., Current understanding of reovirus oncolysis mechanisms. *Oncolytic virotherapy* **2018,** *7*, 53.
4. Clements, D.; Helson, E.; Gujar, S. A.; Lee, P. W., Reovirus in cancer therapy: an evidence-based review. *Oncolytic Virotherapy* **2014,** *3*, 69.
5. Kelly, K.; Nawrocki, S.; Mita, A.; Coffey, M.; Giles, F. J.; Mita, M., Reovirus-based therapy for cancer. *Expert opinion on biological therapy* **2009,** *9* (7), 817-830.
6. Marsh, M.; Helenius, A., Virus entry: open sesame. *Cell* **2006,** *124* (4), 729-740.
7. Delguste, M.; Zeippen, C.; Machiels, B.; Mast, J.; Gillet, L.; Alsteens, D., Multivalent binding of herpesvirus to living cells is tightly regulated during infection. *Science advances* **2018,** *4* (8), eaat1273.
8. Koehler, M.; Delguste, M.; Sieben, C.; Gillet, L.; Alsteens, D., Initial step of virus entry: virion binding to cell-surface glycans. *Annu Rev Virol* **2020,** *7* (1), 143-165.
9. Reiter, D. M.; Frierson, J. M.; Halvorson, E. E.; Kobayashi, T.; Dermody, T. S.; Stehle, T., Crystal structure of reovirus attachment protein σ1 in complex with sialylated oligosaccharides. *PLoS pathogens* **2011,** *7* (8), e1002166.
10. Chappell, J. D.; Prota, A. E.; Dermody, T. S.; Stehle, T., Crystal structure of reovirus attachment protein σ1 reveals evolutionary relationship to adenovirus fiber. *The EMBO journal* **2002,** *21* (1-2), 1-11.
11. Dietrich, M. H.; Ogden, K. M.; Long, J. M.; Ebenhoch, R.; Thor, A.; Dermody, T. S.; Stehle, T., Structural and functional features of the reovirus σ1 tail. *Journal of virology* **2018,** *92* (14), e00336-18.
12. Reiss, K.; Stencel, J. E.; Liu, Y.; Blaum, B. S.; Reiter, D. M.; Feizi, T.; Dermody, T. S.; Stehle, T., The GM2 glycan serves as a functional coreceptor for serotype 1 reovirus. *PLoS pathogens* **2012,** *8* (12), e1003078.
13. Barton, E. S.; Forrest, J. C.; Connolly, J. L.; Chappell, J. D.; Liu, Y.; Schnell, F. J.; Nusrat, A.; Parkos, C. A.; Dermody, T. S., Junction adhesion molecule is a receptor for reovirus. *Cell* **2001,** *104* (3), 441-451.
14. Koehler, M.; Aravamudhan, P.; Guzman-Cardozo, C.; Dumitru, A. C.; Yang, J.; Gargiulo, S.; Soumillion, P.; Dermody, T. S.; Alsteens, D., Glycan-mediated enhancement of reovirus receptor binding. *Nature communications* **2019,** *10* (1), 1-14.
15. Kirchner, E.; Guglielmi, K. M.; Strauss, H. M.; Dermody, T. S.; Stehle, T., Structure of reovirus σ1 in complex with its receptor junctional adhesion molecule-A. *PLoS pathogens* **2008,** *4* (12), e1000235.
16. Stettner, E.; Dietrich, M. H.; Reiss, K.; Dermody, T. S.; Stehle, T., Structure of serotype 1 reovirus attachment protein σ1 in complex with junctional adhesion molecule A reveals a conserved serotype-independent binding epitope. *Journal of virology* **2015,** *89* (11), 6136-6140.

17. Dryden, K. A.; Wang, G.; Yeager, M.; Nibert, M. L.; Coombs, K. M.; Furlong, D. B.; Fields, B. N.; Baker, T. S., Early steps in reovirus infection are associated with dramatic changes in supramolecular structure and protein conformation: analysis of virions and subviral particles by cryoelectron microscopy and image reconstruction. *The Journal of cell biology* **1993,** *122* (5), 1023-1041.
18. Furlong, D. B.; Nibert, M.; Fields, B., Sigma 1 protein of mammalian reoviruses extends from the surfaces of viral particles. *Journal of virology* **1988,** *62* (1), 246-256.
19. Alsteens, D.; Newton, R.; Schubert, R.; Martinez-Martin, D.; Delguste, M.; Roska, B.; Müller, D. J., Nanomechanical mapping of first binding steps of a virus to animal cells. *Nature nanotechnology* **2017,** *12* (2), 177-183.
20. Bustamante, C.; Marko, J. F.; Siggia, E. D.; Smith, S., Entropic elasticity of λ-phage DNA. *Science* **1994,** *265* (5178), 1599-1600.
21. Evans, E. A.; Calderwood, D. A., Forces and bond dynamics in cell adhesion. *Science* **2007,** *316* (5828), 1148-1153.
22. Evans, E.; Ritchie, K., Dynamic strength of molecular adhesion bonds. *Biophysical journal* **1997,** *72* (4), 1541-1555.
23. Rankl, C.; Kienberger, F.; Wildling, L.; Wruss, J.; Gruber, H. J.; Blaas, D.; Hinterdorfer, P., Multiple receptors involved in human rhinovirus attachment to live cells. *Proceedings of the National Academy of Sciences* **2008,** *105* (46), 17778-17783.
24. Verdorfer, T.; Bernardi, R. C.; Meinhold, A.; Ott, W.; Luthey-Schulten, Z.; Nash, M. A.; Gaub, H. E., Combining in vitro and in silico single-molecule force spectroscopy to characterize and tune cellulosomal scaffoldin mechanics. *Journal of the American Chemical Society* **2017,** *139* (49), 17841-17852.
25. Phillips, J. C.; Hardy, D. J.; Maia, J. D.; Stone, J. E.; Ribeiro, J. V.; Bernardi, R. C.; Buch, R.; Fiorin, G.; Hénin, J.; Jiang, W., Scalable molecular dynamics on CPU and GPU architectures with NAMD. *The Journal of chemical physics* **2020,** *153* (4), 044130.
26. Izrailev, S.; Stepaniants, S.; Balsera, M.; Oono, Y.; Schulten, K., Molecular dynamics study of unbinding of the avidin-biotin complex. *Biophysical journal* **1997,** *72* (4), 1568-1581.
27. Dudko, O. K.; Hummer, G.; Szabo, A., Intrinsic rates and activation free energies from single-molecule pulling experiments. *Physical review letters* **2006,** *96* (10), 108101.
28. Park, S.; Schulten, K., Calculating potentials of mean force from steered molecular dynamics simulations. *The Journal of chemical physics* **2004,** *120* (13), 5946-5961.
29. Melo, M. C.; Bernardi, R. C.; De La Fuente-Nunez, C.; Luthey-Schulten, Z., Generalized correlation-based dynamical network analysis: a new high-performance approach for identifying allosteric communications in molecular dynamics trajectories. *The Journal of Chemical Physics* **2020,** *153* (13), 134104.
30. Melo, M. C.; Gomes, D. E.; Bernardi, R. C., Molecular Origins of Force-Dependent Protein Complex Stabilization during Bacterial Infections. *Journal of the American Chemical Society* **2022,** *145* (1), 70-77.
31. Diller, J. R.; Halloran, S. R.; Koehler, M.; dos Santos Natividade, R.; Alsteens, D.; Stehle, T.; Dermody, T. S.; Ogden, K. M., Reovirus σ1 conformational flexibility modulates the efficiency of host cell attachment. *Journal of Virology* **2020,** *94* (23), e01163-20.
32. Eckhardt, M.; Gotza, B.; Gerardy-Schahn, R., Mutants of the CMP-sialic acid transporter causing the Lec2 phenotype. *Journal of Biological Chemistry* **1998,** *273* (32), 20189-20195.
33. Arnberg, N.; Edlund, K.; Kidd, A. H.; Wadell, G. r., Adenovirus type 37 uses sialic acid as a cellular receptor. *Journal of virology* **2000,** *74* (1), 42-48.

34. Williams, P. M., Analytical descriptions of dynamic force spectroscopy: behaviour of multiple connections. *Analytica Chimica Acta* **2003,** *479* (1), 107-115.
35. Suzuki, K.; Fueyo, J.; Krasnykh, V.; Reynolds, P. N.; Curiel, D. T.; Alemany, R., A conditionally replicative adenovirus with enhanced infectivity shows improved oncolytic potency. *Clinical Cancer Research* **2001,** *7* (1), 120-126.
36. Ruthardt, N.; Lamb, D. C.; Bräuchle, C., Single-particle tracking as a quantitative microscopy-based approach to unravel cell entry mechanisms of viruses and pharmaceutical nanoparticles. *Molecular therapy* **2011,** *19* (7), 1199-1211.
37. Berard, A.; Coombs, K. M., Mammalian reoviruses: propagation, quantification, and storage. *Current protocols in microbiology* **2009,** *14* (1), 15C. 1.1-15C. 1.18.
38. Baer, G. S.; Dermody, T. S., Mutations in reovirus outer-capsid protein sigma3 selected during persistent infections of L cells confer resistance to protease inhibitor E64. *Journal of Virology* **1997,** *71* (7), 4921-4928.
39. Mainou, B. A.; Dermody, T. S., Transport to late endosomes is required for efficient reovirus infection. *Journal of virology* **2012,** *86* (16), 8346-8358.
40. Fecek, R. J.; Busch, R.; Lin, H.; Pal, K.; Cunningham, C. A.; Cuff, C. F., Production of Alexa Fluor 488-labeled reovirus and characterization of target cell binding, competence, and immunogenicity of labeled virions. *Journal of immunological methods* **2006,** *314* (1-2), 30-37.
41. Wildling, L.; Unterauer, B.; Zhu, R.; Rupprecht, A.; Haselgrübler, T.; Rankl, C.; Ebner, A.; Vater, D.; Pollheimer, P.; Pohl, E. E., Linking of sensor molecules with amino groups to amino-functionalized AFM tips. *Bioconjugate chemistry* **2011,** *22* (6), 1239-1248.
42. Ebner, A.; Hinterdorfer, P.; Gruber, H. J., Comparison of different aminofunctionalization strategies for attachment of single antibodies to AFM cantilevers. *Ultramicroscopy* **2007,** *107* (10-11), 922-927.
43. Dupres, V.; Menozzi, F. D.; Locht, C.; Clare, B. H.; Abbott, N. L.; Cuenot, S.; Bompard, C.; Raze, D.; Dufrêne, Y. F., Nanoscale mapping and functional analysis of individual adhesins on living bacteria. *Nature methods* **2005,** *2* (7), 515-520.
44. Butt, H.-J.; Jaschke, M., Calculation of thermal noise in atomic force microscopy. *Nanotechnology* **1995,** *6* (1), 1.
45. Bustamante, C.; Marko, J.; Siggia, E.; Smith, S., Entropic elasticity of lambda-phage DNA. *Proc. Natl. Acad. Sci USA* **1991,** *88*, 10009.
46. Newton, R.; Delguste, M.; Koehler, M.; Dumitru, A. C.; Laskowski, P. R.; Müller, D. J.; Alsteens, D., Combining confocal and atomic force microscopy to quantify single-virus binding to mammalian cell surfaces. *Nature protocols* **2017,** *12* (11), 2275-2292.
47. Rankl, C.; Wildling, L.; Neundlinger, I.; Kienberger, F.; Gruber, H.; Blaas, D.; Hinterdorfer, P., Determination of the kinetic on-and off-rate of single virus–cell interactions. In *Atomic Force Microscopy in Biomedical Research*, Springer: 2011; pp 197-210.
48. Webb, B.; Sali, A., Comparative protein structure modeling using MODELLER. *Current protocols in bioinformatics* **2016,** *54* (1), 5.6. 1-5.6. 37.
49. Jo, S.; Kim, T.; Iyer, V. G.; Im, W., CHARMM-GUI: a web-based graphical user interface for CHARMM. *Journal of computational chemistry* **2008,** *29* (11), 1859-1865.
50. Jorgensen, W. L.; Jenson, C., Temperature dependence of TIP3P, SPC, and TIP4P water from NPT Monte Carlo simulations: Seeking temperatures of maximum density. *Journal of computational chemistry* **1998,** *19* (10), 1179-1186.

51. Ribeiro, J. V.; Bernardi, R. C.; Rudack, T.; Stone, J. E.; Phillips, J. C.; Freddolino, P. L.; Schulten, K., QwikMD—integrative molecular dynamics toolkit for novices and experts. *Scientific reports* **2016,** *6* (1), 1-14.
52. Best, R. B.; Zhu, X.; Shim, J.; Lopes, P. E.; Mittal, J.; Feig, M.; MacKerell Jr, A. D., Optimization of the additive CHARMM all-atom protein force field targeting improved sampling of the backbone ϕ, ψ and side-chain χ1 and χ2 dihedral angles. *Journal of chemical theory and computation* **2012,** *8* (9), 3257-3273.
53. Darden, T.; York, D.; Pedersen, L., Particle mesh Ewald: An N· log (N) method for Ewald sums in large systems. *The Journal of chemical physics* **1993,** *98* (12), 10089-10092.
54. Silverman, B. W., *Density estimation for statistics and data analysis*. Routledge: 2018.
55. Humphrey, W.; Dalke, A.; Schulten, K., VMD: visual molecular dynamics. *Journal of molecular graphics* **1996,** *14* (1), 33-38.
56. Connolly, M. L., Solvent-accessible surfaces of proteins and nucleic acids. *Science* **1983,** *221* (4612), 709-713.